J. Condensed Matter Nucl. Sci. 41 (2026) 99–112

Research Article

Multiple Scattering, Coherent Resonance, Quantum Flux and Quantum Hydrogen Energy

Xingzhong Li, Changlin Liang, Si Chen, Jian Tian, Bin Liu, Zhanming Dong, Guisong Huang

Dept. of Physics

Shuxin Zheng

Dept. of Engineering Physics, Tsinghua University, Beijing, CHINA

Abstract

S. E. Koonin's formula and Bethe's calculation on solar energy are combined with the 2-step nuclear resonance caused by multiple scattering in lattice in order to evaluate the resonance effect on the possible low energy nuclear reaction rate. This resonance is justified by the 6 straight lines from 6 laboratories (Fleischmann, Storms, Dennis, Mizuno, Parkhomov, and Tsinghua) in 5 countries. It may explain both Storms' tritium and Miles' correlation between excess power and ^{4}He data. Similar to low energy electron diffraction, the low energy proton diffraction has 3 effects: (1) turns 2-body phase-shift into many-body phase-shift and makes coherent resonance in lattice, i.e. puts many peaks of wave function at many nuclear surfaces simultaneously and replaces the Gamow suppression by Boltzmann factor; (2) many bouncing back and forth motions between interface of 2 films greatly enhance the number of nuclear reactions; (3) reduces the total reflection rate from a set of films in terms of interference between many reflected waves; then, confine the incident wave inside the multiple film system for a much longer time. It is consistent with the correlation between quantum diffusion flux and excess power. This model may further explain 5-peak pattern and the $\sqrt[3]{A}$-law in the nuclear transmutation of metal hydrides (Miley, Mizuno, and Ohmori's data). This is the **Lattice Enhanced Nuclear Resonance** (LENR). It is supposed to appear in the "electron screening potential", and show the 5-peak pattern as well. 3 experiments are suggested to verify this possible nuclear origin in electron screening potential. It may turn metal-hydride a fuel burning with hydrogen together, rather than a furnace for burning hydrogen in it.
 ISSN 2227-3123

Keywords: Koonin's formula, multiple scattering, coherent resonance, lattice enhanced nuclear resonance, 5-peak pattern in electron screening potential, correlation between quantum diffusion flux and excess power, Gamow suppression and Boltzmann factor, low energy electron diffraction, Many-body phase-shift.

1. Introduction

Thirty-six years ago, we learned that cold fusion produces excess heat. A few years later we learned that excess heat is correlated with deuterium flux. Now we understand that there are two kinds of flux: classical flux and quantum flux.

 ISSN 2227-3123

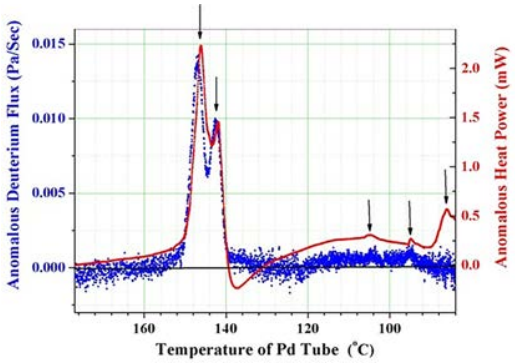

Figure 1. Correlation between anomalous deuterium flux and anomalous heat flow.

Classical flux arises from two-body collisional diffusion, whereas quantum flux results from wave scattering by many bodies in a lattice (i.e., multiple scattering). The excess power is only correlated with this quantum flux. Classical flux decreases with temperature monotonically, but quantum flux has many peaks when the temperature is decreasing. In Fig. 1 the blue line shows the anomalous deuterium flux passing through a thin wall of a Pd tube [1]. When the temperature of the tube drops from $\sim$180° C to 80° C, the blue line shows many peaks instead of monotonic behavior. We will discuss why there are peaks in anomalous deuterium flux due to multiple scattering, and why these peaks are correlated with excess power due to the wave function peak at the nuclear surface. Then we will propose experimental tests of our model.

2. Quantum Flux Passing Many Films: Wave Superposition and Interference

Wave has a phase, and the superposition principle may lead to partial or complete cancellation of the wave's amplitude. Thus, wave mechanics may explain the peak behavior of transmission. This is the advantage of quantum flux over classical flux. In quantum mechanics, we are dealing with the wave function, ψ first, instead of dealing with the observable quantities directly such as flux, transmission rate, T, and reflection rate, R. We define the incoming and outgoing wave functions as a linear combination of the forward, e^{ikz}, and backward, e^{-ikz}, plane waves in upper plot of Fig. 2:

$$\psi_L = U_L^+ e^{ikz} + U_L^- e^{-ikz}; \tag{1}$$

$$\psi_R = U_R^+ e^{ikz} + U_R^- e^{-ikz}. \tag{2}$$

The matrix, $M[1]$, is used to describe the wave scattering by a thin film:

$$\begin{bmatrix} U_L^+ \\ U_L^- \end{bmatrix} = M[1] \cdot \begin{bmatrix} U_R^+ \\ U_R^- \end{bmatrix} \equiv \begin{bmatrix} m_{11}\ m_{12} \\ m_{21}\ m_{21} \end{bmatrix} \cdot \begin{bmatrix} U_R^+ \\ U_R^- \end{bmatrix}. \tag{3}$$

When there is more than one thin film, the reflected wave by the first film may superpose on the reflected wave from the second film…etc. They may interfere with each other and may even be cancelled to zero amplitude. This is the origin of the peak behavior in quantum flux. It may be described by matrix algebra as follows. $M\,[N]$, which

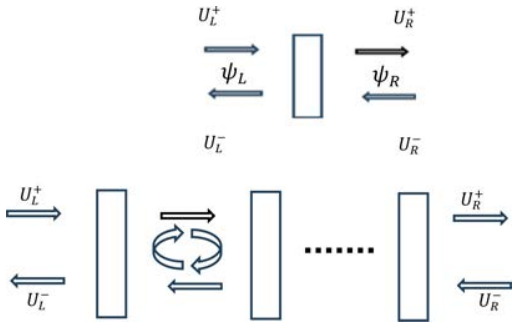

Figure 2. Incoming, outgoing, and reflected waves for a single film (upper) and multiple films (lower).

describes the scattering by N films, may be expressed in terms of the single film parameters as:

$$M[N] \equiv \underbrace{M[1] \cdot M[1] \cdots M[1]}_{N} \equiv \begin{bmatrix} M[N]_{11} & M[N]_{12} \\ M[N]_{21} & M[N]_{22} \end{bmatrix}; \tag{4}$$

$$M[N]_{11} = \frac{Sin[N\alpha]}{Sin[\alpha]} m_{11} - \frac{Sin[(N-1)\alpha]}{Sin[\alpha]}; M[N]_{21} = \frac{Sin[N\alpha]}{Sin[\alpha]} m_{21}; \tag{5}$$

$$\alpha = ArcCos\left[\frac{m_{11}+m_{22}}{2}\right]; \tag{6}$$

The observable physical quantities (reflection rate $R[N]$, transmission rate $T[N]$) are related to the square of the absolute value of these coefficients in the wave functions (1) and (2):

$$R[1] \underbrace{=}_{when\ U_R^-=0} \left|\frac{U_L^-}{U_L^+}\right|^2 = \left|\frac{m_{21}}{m_{11}}\right|^2; \qquad T[1] \underbrace{=}_{when\ U_R^-=0} \left|\frac{U_R^+}{U_L^+}\right|^2 = \left|\frac{1}{m_{11}}\right|^2; \tag{7}$$

$$R[N] \underbrace{=}_{when\ U_R^-=0} \left|\frac{U_L^-}{U_L^+}\right|^2 = \left|\frac{M[N]_{21}}{M[N]_{11}}\right|^2; \quad T[N] \underbrace{=}_{when\ U_R^-=0} \left|\frac{U_R^+}{U_L^+}\right|^2 = \left|\frac{1}{M[N]_{11}}\right|^2. \tag{8}$$

Using Eq. (5), we have:

$$R[N] = \left|\frac{M[N]_{21}}{M[N]_{11}}\right|^2 = \left|\frac{Sin[N\alpha]\ m_{21}}{Sin[N\alpha]\ m_{11} - Sin[(N-1)\alpha]}\right|^2; \tag{9}$$

$$T[N] = \left|\frac{1}{M[N]_{11}}\right|^2 = \left|\frac{Sin[\alpha]}{Sin[N\alpha]\ m_{11} - Sin[(N-1)\alpha]}\right|^2. \tag{10}$$

Even if the reflection rate of a single film is not zero ($m_{21} \neq 0$), the reflection rate of N films may still be zero, as long as $Sin[N\alpha] = 0$. This is due to the interference among the reflected waves. When all the films are elastic films, $R[N] = 0$ must come with a perfect transmission, i.e., $T[N]$ =1. It implies there are many reflections and transmissions between films. Of course, these motions bouncing back and forth are favorable for enhancing the interactions of incoming wave with the target nuclei in each film. Particularly, when the many-body phase-shift, $\delta_m = \frac{\pi}{2}$, the peak of the wave function may reach the surface of the target nucleus. It will further increase the interaction between the incoming wave and target nucleus and enhance the quantum transition probability—the resonant quantum transition.

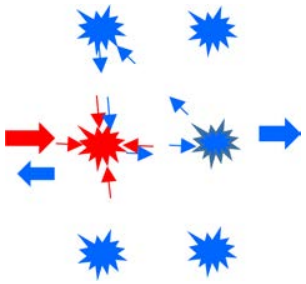

Figure 3. Primary injected wave (red) and secondary scattered wave (blue).

3. The Resonance in a Single Film: 2-Body Phase-Shift δ_2 and Many-Body Phase-Shift δ_m

Multiple scattering happens not only between films, but also inside each film**.** The primary injected wave will be scattered by many scatterers in a film. In Fig. 3, the red incident plane wave will be decomposed to many spherical waves around many scatterers. Each incoming spherical wave will be scattered by an individual scatterer and produce the blue scattered spherical waves. The blue scattered wave will propagate inside the film and will be scattered by other scatterers in the lattice. At thermal energy, the wavelength of the deuteron is 1.3 Å, which is comparable with the crystal constant (palladium's crystal constant is 3.89 Å). Thus, there may be interference between the incident wave and scattered wave as well. This interference may lead to the many-body phase shift, $\delta_m = \frac{\pi}{2}$, even if the 2-body phase shift, $\delta_2 \neq \frac{\pi}{2}$. The wave function of 2-body scattering in quantum mechanics, ψ_2, is expressed by a linear combination of plane wave in z-direction, and a spherical outgoing wave scattered by the scatterer at point $r = 0$:

$$\psi_2 \approx e^{i\,k\,z} + f(\theta,\varphi)\frac{e^{i\,k\,r}}{r}. \tag{11}$$

Many-body scattering in a single film is expressed by:

$$\psi_{ms} \approx \sum_s \{e^{i\,k\cdot r_s} + f(\theta,\varphi)\frac{e^{i\,k\,r_s}}{r_s}\}. \tag{12}$$

Here, ψ_{ms} is the summation of incoming waves and scattered waves around each scatterer at every lattice point, $\boldsymbol{R_s}$. $\boldsymbol{k}$ **i**s the wave vector in various directions (k is its magnitude).

$$\boldsymbol{r_s} \equiv \boldsymbol{r} - \boldsymbol{R_s}. \tag{13}$$

$\boldsymbol{r_s}$ is the radius from one scatterer at one of lattice points at $\boldsymbol{R_s}$. Because many scatterers interact with one another, the resulting wave dynamics become highly complex. Fortunately, the electron screening simplifies the situation. Low energy electron diffraction (LEED) assumes a muffin-tin-like potential to describe the potential field [2]. It means that the individual scatterer would not change the potential field of other scatterers, the only change is due to the change of the boundary condition. In 2-body scattering, the scattered wave function propagates to infinity where the potential field is zero. However, in the case of many-body scattering the scattered wave function would meet a lot of boundaries which are the surfaces of other muffin-tins. In 2-body scattering, we use the phase-shift, δ_2, to describe the effect of boundary on the wave function. During the scattering, the incoming plane wave has to be decomposed into many spherical waves with different angular momentum, *l*, because the interaction between the wave and scatterer varies for

different angular-momentum due to the variation of the "collimate distance" at one scatterer:

$$e^{i\,k\cdot r_s} = \sum_{l,m} 4\pi i^l (-1)^m Y_{l,m}(\Omega_k) j_l(kr_s) Y_{l,m}(\Omega_{r_s}). \tag{14}$$

Here, $j_l(kr_s)$ is the spherical Bessel function. It describes the free motion of the proton outside the muffin-tin region in the film. It is important to notice that

$$j_l(kr) \xrightarrow{kr\ll 1} \frac{(kr)^l}{(2l+1)!!}. \tag{15}$$

It implies that at low energy, the S-wave (*l=0*) would be dominant in the summation (14) because the momentum of deuteron, *k*, is very small. Hence, we may keep S-wave only in our qualitative discussion. This will further simplify the complicated situation. Otherwise, *m* would run over *-l, -(l-1), -(l-2),…(l-1), l* and *l* would run over all integer numbers from 0 to ∞. $Y_{l,m}(\Omega_k)$ and $Y_{l,m}(\Omega_r)$ are the spherical functions in the direction of ***k*** and ***r.*** When *r* is far away from the muffin-tin [2],

$$j_l(kr) \xrightarrow{kr\gg 1} \frac{Sin[kr - \frac{l\,\pi}{2}]}{kr}. \tag{16}$$

It corresponds to a spherical wave in and a spherical wave out without any phase-shift, i.e. $\delta_2 = 0$. Indeed, the muffin-tin potential would change the wave function, and have an additional outgoing spherical wave $h_l^{(1)}(kr)$. $h_l^{(1)}(kr)$ is the first kind of spherical Hankel function, and has the desired asymptotic behavior as a spherical outgoing wave:

$$h_l^{(1)}(kr) \xrightarrow{kr\gg 1} \frac{(-i)^l}{i\,kr} e^{i((kr-\frac{l\pi}{2})}(1 + \frac{il\,(l+1)}{2kr}). \tag{17}$$

It just has the form of the second term in eq. (12). Thus,

$$\psi_{ms} \approx \sum_s e^{i\,k\cdot r_s} + f\,(\theta,\varphi)\,\frac{e^{i\,k\,r_s}}{r_s} = \sum_{s,l,m} \{4\pi i^l (-1)^m Y_{l,m}\,(\Omega_k)\,[j_l\,(kr_s) + t_l\,h_l^{(1)}(kr_s)] Y_{l,m}\,(\Omega_{r_s})\}. \tag{18}$$

When multiple scattering is ignored, the coefficient of the linear combination, t_l , may be expressed by 2-body phase-shift, δ_{2l}, as [2]:

$$t_{2l} = ie^{i\delta_{2l}} Sin[\delta_{2l}]. \tag{19}$$

For low energy deuteron, only the S-wave is kept,

$$\psi_{ms} \approx \sum_s \{4\pi Y_{0,0}\,(\Omega_k)\,[j_0(kr_s) + t_{20} h_0^{(1)}(kr_s)] Y_{0,0}(\Omega_{r_s})\}; \tag{20}$$

$$t_{20} = ie^{i\delta_{20}} Sin[\delta_{20}]. \tag{21}$$

Here, δ_{20} is defined as 2-body phase-shift with S-wave only. When the other scatterers' effect is included, δ_{20} in t_{20} would be replaced by many-body phase-shift, δ_{m0}.

$$t_{m0} = ie^{i\delta_{m0}} Sin[\delta_{m0}]; \tag{22}$$

$$t_{m0} = \frac{t_{20}}{1 - G_{ST} t_{20}}. \tag{23}$$

Eq. (23) shows the many-body phase-shift, δ_{m0}, in terms of 2-body phase-shift, δ_{20}, and G_{ST}. G_{ST} includes all the effects from all the scattered waves from all other scatterers. In the low energy electron diffraction theory [2] G_{ST}

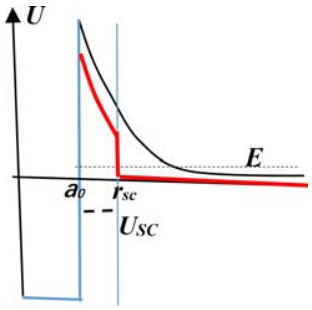

Figure 4. The silo-like potential with electron screening (Red line).

is called the structure factor which is a factor to show the feed-back effect of the scattered wave, $h_0^{(1)}(kr_s)$. When the scattered wave $h_0^{(1)}(kr_s)$ is leaving one scatterer, it becomes incoming waves for all other scatterers inside the film. Every other scatterer would scatter this secondary incoming wave, and produce the third scattered wave which may feed-back to the first scatterer (the red one in Fig. 3). Then, this feed-back incoming wave would be scattered by the red scatterer again. This superposition of waves would continue to form an infinite geometric series with a common ratio, $(G_{ST} \cdot t_{20})$. The details about crystal structure factor, G_{ST}, may be found in any LEED book. Our interest is that G_{ST} will make the many-body phase-shift, $\delta_{m0} = \frac{\pi}{2}$, even if 2-body phase-shift, $\delta_{20} \neq \frac{\pi}{2}$. This is the key point of Lattice Enhanced Nuclear Resonance—The resonance induced by multiple scattering.

When $\delta_{m0} = \frac{\pi}{2}$, $t_{m0} = -1$; then

$$\psi_{ms} \approx \sum_s \{4\pi Y_{0,0}(\Omega_k)[j_0(kr_s)+t_{m0}h_0^{(1)}(kr_s)]Y_{0,0}(\Omega_{r_s})\} = \sum_s \{4\pi Y_{0,0}(\Omega_k)[j_0(kr_s)-h_0^{(1)}(kr_s)]Y_{0,0}(\Omega_{r_s})\}$$
$$= \sum_s \{4\pi Y_{0,0}(\Omega_k)[j_0(kr_s)-(j_0(kr_s)+in_0(kr_s)]Y_{0,0}(\Omega_{r_s})\} = \sum_s \{4\pi Y_{0,0}(\Omega_k)[-in_0(kr_s)]Y_{0,0}(\Omega_{r_s})\}. \quad (24)$$

Eq. (24) shows the cancellation of incoming $j_0(kr_s)$ due to interference. $n_0(kr_s)$ is the spherical Neumann function. Its amplitude has the desired behavior—peaked at the muffin-tin surface where kr_s<<1:

$$n_0(kr_s) = -\frac{Cos[kr_s]}{kr_s}; \quad (25)$$

Now, the question is if this spherical Neumann function would be connected to the irregular Coulomb wave function, $\frac{G_0(kr_s)}{kr_s}$, which is the necessary condition to create a mother state for a resonant transition to the daughter state as we proposed in 2-step nuclear resonance model [3], [4].

4. The Connection of the Wave Function at the Interface Between Coulomb Field and Zero-Field Regions

In multiple scattering model, the potential field outside the electron screening region ($r > r_{SC}$ in Fig. 4) and inside the silo-like region ($a_0 < r < r_{SC}$ in Fig. 4) are shown by red line. The electron screening effect has been treated as an electron screening potential, U_{SC}, which accelerates the incoming positive ion. Indeed, the incident proton energy (E) is conserved in a static electrical field, but its momentum (k_c) inside the down-shifted Coulomb field equals to $\sqrt{\frac{2\mu(E-\frac{Ze^2}{4\pi\varepsilon_0 r}+U_{SC})}{\hbar^2}}$, and its momentum outside the silo-like region (k) equals to $\sqrt{\frac{2\mu E}{\hbar^2}}$. $\hbar$ is the reduced Planck Constant, μ is the reduced mass of the deuteron, ε_0 is the dielectric constant of vacuum, Ze is the electrical charge

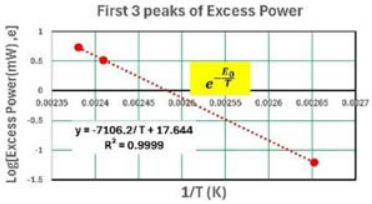

Figure 5. The Boltzmann factor is confirmed by the first 3 points in Fig 1.

of the screening material, U_{SC} is the electron screening potential. Hence, inside the silo-like region the irregular Coulomb function, $G_0(\rho,\eta) \equiv G_0\left(k_C r, \frac{1}{k_C a_C}\right)$. Here, $a_C \equiv \frac{4\pi\varepsilon_0\hbar^2}{\mu Z e^2}$. In order to make a smooth connection between $\frac{G_0(kr_s)}{kr_s}$ and $(-\frac{Cos[kr_s]}{kr_s})$ at the interface face ($r = r_{SC}$ in Fig. 4), we have to check if both of them have the same sign for their logarithmic derivative. The logarithmic derivative of $G_0\left(k_C r, \frac{1}{k_C a_C}\right)$ is negative in the region where E is less than the potential energy. However, $Cos\,[kr_s\,]$ has a negative logarithmic derivative only in the region $kr_s < \frac{\pi}{2}$. In LEED, the radius of muffin-tin potential is not strictly defined. Only the phase-shift, δ_2, plays an important role in its effect on other scatterers. If we assume the radius of the silo-like potential, r_{SC}, is in the order of 10^{-14} m, which is less than the radius of the innermost orbit of the electrons for screening material, but is still greater than the nuclear radius of the screening material; then, $k < \frac{\pi}{2r_{sc}}$ for all "cold fusion" experiments which were done at temperature lower than 2000°C. Thus it is sure that the wave function in the zero-field region would be smoothly connected to $G_0\left(k_C r, \frac{1}{k_C a_C}\right)$ at interface, when the phase-shift for multiple scattering, $\delta_{m0} = \frac{\pi}{2}$. In other words, the wave function, $n_0\,(kr_s)$, would be connected to $G_0\left(k_C r_S, \frac{1}{k_C a_C}\right)$ at interface and makes a peak at the surface of the nucleus of the screening material. This peak-wise wave function produced by multiple elastic scattering within the lattice constitutes the initial state for a transition to the final state (a bound state) to produce the excess power. This excess power is much greater than that in the non-resonance case where the peak of the initial wave function is outside of Coulomb barrier region ($\delta_{m0} \neq \frac{\pi}{2}$). In Appendix, we have shown that the wave function peak at nuclear surface would turn Gamow factor ($e^{-\frac{3380}{T^{1/3}}}$) into Boltzmann factor ($e^{-\frac{E_0}{k_B T}}$). Here, E_0 is the resonance energy, k_B is the Boltzmann constant, T is the temperature in Kelvin. This ($e^{-\frac{E_0}{k_B T}}$) factor is confirmed by the experimental data for the first 3 points in Fig. 1 (see Fig. 5, the effect of heat of formation on heat flow for deuteride in Pd has been deducted.) This temperature-dependence, $e^{-\frac{E_0}{k_B T}}$, has been found in 6 labs of 5 countries [5] as well. Indeed, the slope in Fig. 5 (-7106.2K) is close to that in Pd-D gas loading experiment (-6507.5K) at Tsinghua University [5].

5. Possible Nuclear Reactions at Resonance

When resonance puts the projectile at the surface of target nucleus, there are 2 possible nuclear interactions suggested by experimental results: the weak interaction [6] and the strong interaction [7]. As Bethe pointed out for p+p reactions [8], d+d reaction may produce ^4T through the K-electron capture first; then, ^4T may decay to ^4He. This weak interaction might not affect the calorimetric measurement due to the small coupling constant (see Appendix), and the possible neutrino emission. On the other hand Miles' helium and excess heat correlation measurements show that the strong interaction might produce ^4He directly. S.E. Kooning [9] proposed a method to evaluate the reaction rate by

$$\Lambda = A\ |\Psi_d(a_0)|^2 \tag{26}$$

Here, $A = 1.5 \times 10^{-16} cm^3 s^{-1}$ for $d+d \rightarrow {}^3He + n \oplus {}^3T + p$ reactions. $\Psi_d(a_0)$ is the value of the wave function at the nuclear surface for d+d relative motion(in unit of $cm^{3/2}$). When the reaction rate, Λ, is averaged over Maxwellian distribution using (A14), we have

$$< \Lambda >= A\, I_{resonance} = A * (\frac{\mu}{2\pi k_B T})^{\frac{3}{2}} \left(\frac{a_c}{a_0}\right)^2 \frac{e^2}{4\pi\varepsilon_0 \hbar} \frac{1}{\mu} e^{-\frac{E_0}{k_B T}} \frac{2\pi}{C_2} \tag{27}$$

C_2 is the parameter which determines the energy dependence of the phase shift [4]. Using the **method** in Appendix of reference [4] we have $C_2 = 0.254 keV^{-1}$ for $d + d \rightarrow {}^3He + n \oplus {}^3T + p$ reaction in CM system. From Fig. 5, $E_0 = 7106.2\ K$, and from Fig. 1, T= $414.5\ K$. Eq. (27) gives $< \Lambda > = 1.2 \times 10^{-14} cm^3 s^{-1}$. This reaction rate is for an incident deuteron plane wave normalized to per unit density at infinity. In order to compare with the experimental result in Fig. 1, we need the information about the deuteron flux incident on trapped deuteron in Pd lattice. The deuteron diffusion flux is mainly due to the classical 2-body scattering on the Pd atoms, only the multiple scattering on trapped deuterons may introduce the quantum flux peaks. From Fig. 1, the pressure in the reaction cell changes 0.015 Pa/sec at the first peak. It gives an anomalous flux of $\sim 10^{13}$ deuterons $cm^{-2} s^{-1}$ passing through the thin wall of a Pd tube in a 12.5 ml reaction cell. The thermal speed of the deuteron at 414.5K is $1.85 \times 10^5 cm{\cdot}s^{-1}$. It implies a deuteron density of 10^8 cm^{-3} which is from the multiple scattering on the trapped deuterons. The Pd tube volume is $2.6cm \times \phi 0.4cm \times 0.01cm = 0.033 cm^3$. The deuteron loading ratio is ~0.01 at 414.5K and 1.4 atm; hence, the number of the trapped deuterons is $\sim 10^{18}$. Hence, the resonance d+d reaction rate in Pd tube is $\sim 10^{12} s^{-1}$. It implies a measurable excess power at the level of 1 W. Consider the fact that not all the trapped deuterons are involved in this resonant multiple scattering. It seems consistent with the experimental result of 2 mW.

6. The Possible Resonance During the Hopping Process

The application of multiple scattering requires three conditions [10]: (1) The wave length of incident particles is comparable with the crystal constant; (2) The 2-body interaction potential well of the scatterers should not be overlapped each other. There must be a region to separate the individual potential well; (3) There is enough time to have a resonance before the hopping process to destroy this resonance. It seems possible to satisfy these conditions. The de Broglie wave length of a thermal deuteron is about 1 Å, which is comparable with the Pd crystal constant 3.89 Å. The electron screening might provide the separation among the individual potential wells of the scatterers. The phase speed of the thermal deuteron is about $10^5 cm{\cdot}s^{-1}$. It takes $10^{-13} s$ to travel forth and back between the scatterers in the lattice. This travelling time is much shorter than the hopping time (about 100ps [11]). If the quantum transition to a lower state happens before the hopping process, this resonance would be able to enhance this transition. Hagelstein's group [12] has analysed the transition, and answered the question about the gamma radiation as well.

7. The Bouncing Back and Forth Motion Between Thin Films

The reflections between the coating films play a critical role in most of "cold fusion" experiments, because the reflections enhance the total flux. It explains not only the excess power, but also the correlation between the anomalous flux and the excess power. A measurement of the reflection number between the films before the penetration to the next film is the ratio of reflection rate to transmission rate. Using eq. (7), $\frac{R[1]}{T[1]} = |m_{21}|^2$. $|m_{21}|^2$ is calculated in low energy electron diffraction (LEED) theory. It is directly related to many-body phase shift. It is complicated; however, for the case of S-wave dominant in low energy, there is a simple relation based on Optical Theorem. The imaginary part of the forward scattering amplitude, $f\,(0)$, is related to cross-section, σ_0 , and phase shift, δ_0, as

$$Im\,[f\,(0)] = \frac{k}{4\pi}\sigma_0 = \frac{1}{k}\,(Sin[\delta_0])^2\,. \tag{28}$$

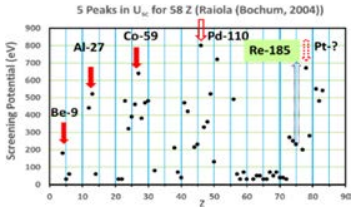

Figure 6. 5-peak pattern in electron screening potential (red arrows).

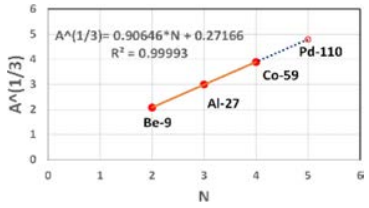

Figure 7. $A^{1/3}$-Plot for the first 3 peaks in U_{SC}.

When $\delta_0 = \frac{\pi}{2}$, $Im\left[f\left(0\right)\right]$ reaches its maxima, and $Re\left[f\left(0\right)\right] = \frac{1}{k}Sin\left[\delta_0\right]Cos\left[\delta_0\right] = 0$. It means that the amplitude of forward scattering, $\left|f\left(0\right)\right|$, takes maxima at $\delta_0 = \frac{\pi}{2}$. Since the S-wave is isotropic, so, the back scattering amplitude $f\left(\pi\right)$ takes its maxima as well. Hence when the multiple scattering makes many-body phase shift, $\delta_{m0} = \frac{\pi}{2}$, it also makes $\left|m_{21}\right|^2$ of a single film maximum. Thus, the bouncing back and forth number is maximized while the wave function peak reaches the nuclear surface. For the multiple film case, when we observe the transmission rate, $T[N]$, has a maxima, the corresponding reflection rate, $R\left[N\right] = 1 - T[N]$ is minimized. This implies good confinement in multiple films. It means there will be a lot of bouncing back and forth motions between 2 films before entering the next slot, and it maximizes the number of multiple scatterings. Consequently, the maximum nuclear reaction rate is correlated with the maximum transmission rate as shown by Fig. 1.

8. Multiple Scattering in Electron Screening Experiment

A thin film coating of screening material on a metal substrate is done in all the electron screening experiments. The multiple scattering between this screening material and the substrate might happen when the injected deuterons are slowing down. In Fig. 6 red arrows show a 5-peak pattern in atomic charge number (Z) for electron screening potential, U_{SC}. Prof. Kasagi [13] pointed out that these peak values need an additional mechanism to be explained. Prof. Nagel discovered [14] the similarity between the 5-peak pattern in nuclear transmutation of metal hydrides and in U_{SC}. The multiple scattering might provide an additional reason for the nuclear origin of this 5-peak pattern, because the 2-body phase shift, δ_{20}, in eq. (21) is determined by the boundary condition at the nuclear surface. It should have periodicity in atomic mass number (A). Fig. 7 is the $A^{1/3}$-plot for the first 3 peaks in Fig. 6. Be-9, Al-27, Co-59 are closely on a straight line. It may be extended to the 4-th peak Pd-110, which is in good agreement with Fig. 6. To verify its nuclear origin, we may run the electron screening experiment again using enriched Pd-110 to see if there is any increase in U_{SC}, because the abundance of Pd-110 in natural Pd is only 11.7%. Or, we may detect whether there is any characteristic radiation from Pd-111 in the nuclear product (2.23 MeV $\beta-$radiation with $T_{1/2}$ ~24min. from Pd-111G, and 170 keV $\gamma-$radiation with $T_{1/2}$ ~5.5 hours from Pd-111m) [15]. Iwamura's early device for nuclear transmutation might be used to test if there is any peak flux near 147°C. This can be done by holding that

temperature for 17 hours; and then immediately detecting these characteristic β and γ radiations. The positive results of these proposed experiments would confirm not only this coherent resonance mechanism, but also solve the puzzle of missing neutrino or gamma radiation in "cold fusion" because Pd-111G ($5/2^+$) and Pd-111m ($11/2^-$) are high spin nuclei with different parities. Only in many-body coherent quantum transition they might be produced at low energy. This would be compelling evidence of lattice enhanced nuclear resonance.

9. Conclusion

There are 2 kinds of flux. Only the quantum flux caused by multiple scattering is correlated with excess power. The multiple scattering provides an initial mother state for Bethe's weak interaction transition or for Oppenheimer's strong interaction transition. Multiple scattering in lattice has 3 effects: (1) turns a group of 2-body phase shift into many-body phase shift for coherent nuclear resonance; (2) bouncing back and forth motion between thin films enhances the effective incoming flux for coherent quantum transitions; (3) reduces the reflection rate at the surface of multiple films to further enhance the effective incoming flux. It appears as a correlation between quantum flux and anomalous excess power. ***This coherent resonance turns a metal hydride into a fuel burning with hydrogen, rather than a furnace for burning hydrogen in it***. It is a ***Lattice Enhanced Nuclear Reaction.*** It shows a bright future for a quantum hydrogen energy.

Acknowledgements

Many thanks to D. Nagel, G. Miley, T. Passell, F. Will, and J. Rothwell for their important assistance.

Appendix. Gamow Factor is Replaced by Boltzmann Factor for Low Energy Nuclear Resonance

In this appendix we will discuss how to modify Bethe's calculation [8] in order to include the case of resonance.

In the resonance integration the contribution from a resonance depends on both its width and height. In eq. (A1) the width is determined by the coefficient, $Tan\,[K]$, and the height is determined mainly by the irregular Coulomb wave function, G (We keep Bethe's notation [8] in this Appendix for comparison). When the phase-shift, K, passes through the resonance point, $\pi/2$, very quickly with the energy reduction, the energy width of a resonance is very narrow. However, if the resonance height, G, also increases very quickly with the energy reduction; then the resonance effect may still remain. Hence, we need to study the energy dependence of both $Tan\,[K]$, and G value near the nuclear surface when $K \to \frac{\pi}{2}$, in order to evaluate its contribution to the resonance integration.

What should be changed to include the case of resonance in Bethe's calculation [8]? The initial wave function of p-p elastic scattering state in the Coulomb field region outside the nuclear potential well was written as:

$$\Psi_p(r) = \frac{e^{iK} Cos\,[K]\ \ (F + Tan\,[K]\ \ G)}{k\ r}. \tag{A1}$$

Here k is the momentum of the relative motion in the c.m. system, r is the distance between the projectile and the target. At low energy,

$$F = C\varrho\Phi(r); \quad G = C^{-1}\Theta(r). \tag{A2}$$

$$C \equiv \sqrt{2\pi\eta}\, e^{-\pi\eta}; \varrho \equiv k\ r, \eta = \frac{e^2}{4\pi\varepsilon_0\hbar v} \equiv \frac{1}{ka_c};\ a_c \equiv \frac{4\pi\varepsilon_0\hbar^2}{\mu e^2}. \tag{A3}$$

Here, C determines the Gamow suppression. ε_0 is the dielectric constant of the vacuum, $\hbar$ is the Planck Constant divided by 2π, v is the relative velocity between the projectile and the target, e is the electric charge of a proton, μ is

the reduced mass of the projectile and the target. $\Phi(\mathrm{r})$ and $\Theta(\mathrm{r})$ are independent of energy, and they are very close to 1 at the surface of nuclear potential ($r = r_0$). Hence, at low energy,

$$Tan\,[K] = -\left[\frac{F\,\frac{1}{F}\frac{\partial F}{\partial r} - \frac{1}{w}\frac{\partial w}{\partial r}}{G\,\frac{1}{G}\frac{\partial G}{\partial r} - \frac{1}{w}\frac{\partial w}{\partial r}}\right]_{r=r_0} = -2\pi\frac{r_0}{a_c}e^{-2\pi\eta}\left[\frac{\frac{1}{F}\frac{\partial F}{\partial r} - \frac{1}{w}\frac{\partial w}{\partial r}}{\frac{1}{G}\frac{\partial G}{\partial r} - \frac{1}{w}\frac{\partial w}{\partial r}}\right]_{r=r_0}. \tag{A4}$$

$Tan\,[K]$ is very small, unless the denominator, $\left[\frac{1}{G}\frac{\partial G}{\partial r} - \frac{1}{w}\frac{\partial w}{\partial r}\right]_{r=r_0} = 0$. Indeed this is just the resonance condition which was not included in Bethe's calculation (w is the wave function inside the nuclear potential well). Bethe assumes K is small (∼0.0017), and replaces $e^{iK}Cos\,[K]$ by 1 in (A1). However, we are considering now the cases including $K \to \frac{\pi}{2}$, the replacement, $e^{iK}Cos\,[K] \to 1$, is no longer valid. Eq. (A1) should be rewritten as:

$$\Psi_p\,(r) = \frac{e^{iK}}{k\,r}\,(Cos\,[K]\;\,F + Sin\,[K]\;\,G) = \frac{e^{iK}}{k\,r}\left(Cos\,[K]\;\,F + \frac{1}{\sqrt{1+(Cot\,[K])^2}}\,G\right) \tag{A5}$$

G is much greater than F at the nuclear surface according to (A2) and (A3). Thus, Bethe still keeps G in (A5) in his non-resonance calculation and calls it "resonance effect". Eq. (A5) is now written as:

$$\Psi_p\,(r) = \frac{e^{iK}}{k\,r}C\varrho\left(Cos[K]\Phi + \frac{1}{\sqrt{1+(Cot\,[K])^2}}C^{-2}\varrho^{-1}\Theta\right) \tag{A6}$$

The energy-dependence of the second term in (A6) is very different between the case of resonance and non-resonance. For the case of no resonance, $(Cot\,[K])^2 \gg 1$:

$$\frac{1}{\sqrt{1+(Cot\,[K])^2}}C^{-2}\varrho^{-1} \approx Tan\,[K]\,C^{-2}\varrho^{-1} = Tan\,[K]\,\frac{e^{2\pi\eta}}{2\pi}\,\frac{a_c}{r_0} \equiv \lambda. \tag{A7}$$

According to (A4), $(Tan\,[K]\,\frac{e^{2\pi\eta}}{2\pi})$ is independent of energy when there is no resonance at low energy. Hence, λ is independent of energy. When the nuclear reaction rate was integrated over the Maxwell distribution of the velocity, the Gamow factor, *C*, in front of $\left(Cos[K]\Phi + \frac{1}{\sqrt{1+(Cot[K])^2}}C^{-2}\varrho^{-1}\Theta\right)$ in (A6) was the only one factor to compete with the Boltzmann factor, $(\frac{\mu}{2\pi k_B T})^{\frac{3}{2}}Exp[-\frac{\mu v^2}{2k_B T}]4\pi v^2 dv$. Here, T is the temperature of the protons, and k_B is the Boltzmann Constant. Since the nuclear reaction rate, $\sigma\,v$, is proportional to the square of the modulus of the wave function; hence, the term involving $|C\;\lambda|^2$ in the integration may be written as:

$$I_{Gamow} = (\frac{\mu}{2\pi k_B T})^{\frac{3}{2}}\int_0^\infty |C\;\lambda|^2\,Exp\left[-\frac{E}{k_B T}\right]\frac{2\pi}{\mu}vdE = (\frac{\mu}{2\pi k_B T})^{\frac{3}{2}}\int_0^\infty |\lambda|^2\,\frac{2\pi\eta}{e^{2\pi\eta}}Exp[-\frac{E}{k_B T}]\frac{2\pi}{\mu}vdE. \tag{A8}$$

Here, $E = \frac{\mu v^2}{2}$ is the kinetic energy. The integrand in (A8) is a product of two factors: an exponentially decreasing $Exp\left[-\frac{E}{k_B T}\right]$, and an exponentially increasing $\frac{1}{e^{2\pi\eta}}$ with E. Their product has a peak at

$$E_G = (\frac{\mu}{2}(\pi\frac{e^2}{4\pi\varepsilon_0\hbar}k_B T)^2)^{\frac{1}{3}}. \tag{A9}$$

Using the steepest descent method, in the case of p-p reaction without resonance Bethe obtained the integration of the famous Gamow peak.

$$I_{Gamow} = 2{*}3^{-\frac{5}{2}}\;(\lambda)^2\;(\frac{3380}{(T)^{\frac{1}{3}}})^2\,(Exp[-\frac{3380}{(T)^{\frac{1}{3}}}]).(T \text{ is in units of Kelvin}) \tag{A10}$$

In the case of resonance, $K \to \frac{\pi}{2}$, $Cot\,[K]^2 \to 0$, $\frac{1}{\sqrt{1+(Cot[K])^2}} \to 1$. The C^{-2} in the coefficient of the second term in (A6) defeats not only the Gamow suppression (C), but also the narrowness of resonance width, when the reaction rate is integrated over the Maxwell distribution of the velocity.

$$I_{resonance} = (\frac{\mu}{2\pi k_B T})^{\frac{3}{2}} \int_0^{\infty} \left| \frac{1}{\sqrt{1+(Cot\,[K])^2}} \left(\frac{e^{2\pi\eta}}{2\pi}\right) \frac{a_c}{r_0} \right|^2 C^2 Exp[-\frac{\mu v^2}{2k_B T}] 4\pi v^2 dv. \tag{A11}$$

Here, we have to carefully consider the energy dependence of the phase shift, K. This information may be extracted from the experimental data of the fusion cross-section at low energy. Based on the Evaluated Nuclear Data Files (ENDF) in the National Nuclear Data Center (NNDC), a comprehensive study of the nuclear fusion cross-sections (see the Appendix in reference [4]) at the low energy showed that for the interaction between two charged nuclei at low energy, $Cot\,[K]$ may be approximated by a product of two factors: a fast changing factor, $(\frac{e^{2\pi\eta}}{2\pi})$, and a slow varying factor, $C_2\,(E-E_0)$:

$$Cot\,[K] = (\frac{e^{2\pi\eta}}{2\pi})\,C_2\,(E-E_0)\,. \tag{A12}$$

Here E_0 is the resonance energy, and C_2 is a constant from p-p elastic scattering data. Therefore.

$$\begin{aligned} I_{resonance} &= (\frac{\mu}{2\pi k_B T})^{\frac{3}{2}} \int_0^{\infty} \left| \frac{1}{\sqrt{1+\left(\left(\frac{e^{2\pi\eta}}{2\pi}\right) C_2\,(E-E_0)\right)^2}} \left(\frac{e^{2\pi\eta}}{2\pi}\right) \frac{a_c}{r_0} \right|^2 \frac{2\pi}{e^{2\pi\eta}} \frac{e^2}{4\pi\varepsilon_0\hbar} Exp[-\frac{\mu v^2}{2k_B T}] 2\pi \frac{1}{\mu} dE \\ &= (\frac{\mu}{2\pi k_B T})^{\frac{3}{2}} \int_0^{\infty} \frac{1}{1+\left(\left(\frac{e^{2\pi\eta}}{2\pi}\right) C_2\,(E-E_0)\right)^2} (\frac{a_c}{r_0})^2 \left(\frac{e^{2\pi\eta}}{2\pi}\right) \frac{e^2}{4\pi\varepsilon_0\hbar} Exp[-\frac{E}{k_B T}] \frac{2\pi}{\mu} dE. \end{aligned} \tag{A13}$$

The integrand of (A13) has a very sharp peak near the energy, E_0, as shown in Fig. A1. The height of the peak is determined by the numerator which is proportional to $\left[e^{2\pi\eta} Exp[-\frac{E}{k_B T}]\right]_{E=E_0}$ and its width is determined by the denominator which is in the order of $\frac{1}{\left(\frac{e^{2\pi\eta}}{2\pi}\right) C_2}$. It is clear that the resonance effect is high enough to overcome the Gamow suppression. Although the width of the resonance peak is decreasing with the resonance energy, E_0, the sharply increasing peak height still contributes enough to overcome both the Gamow suppression and the narrowness of the resonance. The resonance peak acts just like a Delta-function to evaluate the specific value of the integrand after the integration. Using the deepest descent method again:

$$I_{resonance} = (\frac{\mu}{2\pi k_B T})^{\frac{3}{2}} \left(\frac{a_c}{r_0}\right)^2 \frac{e^2}{4\pi\varepsilon_0\hbar} \frac{1}{\mu} e^{-\frac{E_0}{k_B T}} \frac{2\pi}{C_2}. \tag{A14}$$

New features of low energy resonance. The resonance makes G dominant in the linear combination of the wave functions (A1). Hence, *the modulus of the wave function peaks at the surface of nuclear potential well;* and two new features appear:

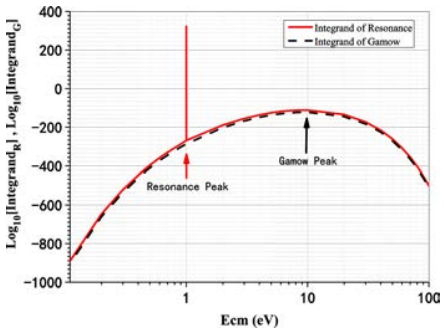

Figure A1. Solid line is the integrand of the resonance integration in (A13). The dashed line is the integrand of the Gamow integration in (A8). E_0=1.0 eV and C_2=0.00164 keV^{-1}. λ=4.80, and T=1000K.

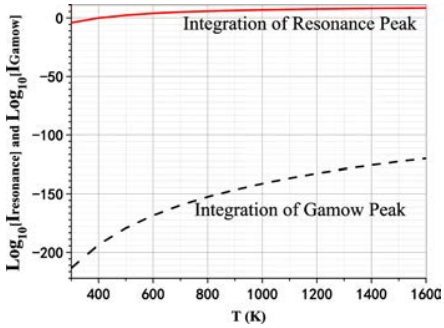

Figure A2. Comparison between the resonance integration $I_{\rm resonance}$ (Solid line) and $I_{\rm Gamow}$ (Dashed line). E_0=1.0 eV, C_2=0.00164 keV^{-1}, λ=4.80.

A. Gamow Suppression Disappears in the Resonance Integration

The Gamow factor is overcome by a resonance even if the resonance is at very low energy. Fig. A1 shows that two integrands in (A8) and (A13) are mostly similar in the logarithmic scale. The big difference appears only in the resonance region around $E = E_0$. When the resonance energy , E_0, is getting lower, the resonance peak height is getting higher as $e^{2\pi\eta}$ while the width of the resonance is getting narrower as $\frac{1}{e^{2\pi\eta}}$. The resonance peak is always high enough to keep the integration of resonance large, overcoming the Gamow suppressing factor. It will enhance the nuclear reaction rate greatly, particularly at low temperatures. Fig. A2 gives the comparison between two integrations $I_{resonance}$ in (A14) and I_{Gamow} in (A10) in logarithmic scale. The solid line is $I_{resonance}$ which is much greater than the I_{Gamow}, shown by the dashed line. The resonance overwhelms the Gamow suppression in the evaluation of the integral $I_{resonance}$.

B. The Evidence of a Low Energy Resonance

The major temperature dependence of the integration of resonance in (A14) is an exponential function, $e^{-\frac{E_0}{k_B T}}$ (The Boltzmann factor). This temperature dependence is a typical straight line in a semi-logarithmic plot, when $\frac{1}{T}$ is used as the abscissa. We may use this exponential dependence to identify a low energy resonance. This dependence has been found in 6 labs in 5 countries [5], and in Fig. 5 as well.

Discussion. Bethe proposed a two-step p-p reaction model: elastic scattering first to form a mother state; then followed by a nuclear transition from the mother state to a daughter state. This model makes low energy resonance feasible in the first step, and is favorable to the second transition to a bound state because the resonance keeps two charged particles closer even if the Coulomb barrier is high and the energy of the projectile is very low.

This model was proposed for p-p reaction; however, it might be applied to the case with higher charge number (Z). We should expect to observe this low energy resonance in a hydrogen-loaded metal as well.

The resonance puts the peak of the wave function at the surface of nuclear potential; hence, it enhances the interaction between the projectile and target. This effect is getting higher when the energy of projectile is getting lower. Indeed, when the energy is much lower than 1 eV, the projectile might be interacting with more than one target nucleus in a crystal of metal. Hence, the multiple scattering must be involved.

Indeed, the reaction rate, $\langle \sigma v \rangle$, in this 2-step model is mainly determined by the volume of the overlapping between the initial and final wave function, and the coupling constant: $(g\, b^3)$. Here g $\sim 10^{-4}$ sec^{-1}, is the Fermi coupling constant for weak interaction in Bethe's solar energy model; b$\sim 10^{-15}$m, is the scale of extension beyond the nuclear potential well for a neutron [8]. Hence $\langle \sigma v \rangle$ for 2-body nuclear fusion is still very small, even if the I_{Gamow} is replaced by $I_{resonance}$. Thus, we have to consider the strong interaction and the multiple scattering effect to enhance further the reaction rate, $\langle \sigma v \rangle$, in order to meet the experimental data.

References

[1] X. Z. Li, B. Liu, J. Tian, Q. M. Wei, R. Zhou, and Z. W. Yu, "Correlation between abnormal deuterium flux and heat flow in a D/Pd system", *J. Phys. D: Appl. Phys*. **36** (2003) 3095–3097.

[2] J. B. Pendry, Low Energy Electron Diffraction, Academic Press, (London and New York) 1974.

[3] X. Z. Li, Z. M. Dong, C. L. Liang, and G. S. Huang. "Resonant Surface Capture Model." *Journal of Condensed Matter Nuclear Science,* **29** (1) 2019: 440–52. https://doi.org/10.70923/001c.72523.

[4] X. Z. Li, C. L. Liang, G. S. Huang, B. Liu, J. Tian, S. Chen, Y. Chen, Z. M. Dong, and S. X. Zheng. 2025. "Cubic Root ($\sqrt[3]{A}$)—Law in Nuclear Transmutation of Metal Hydrides", *Journal of Condensed Matter Nuclear Science*, **39** (March,2024):322–45. https://doi.org/10.70923/001c.134020.

[5] D. J. Nagel, "Experimental Status of LENR", *ARPA-E Workshop on Low-Energy Nuclear Reactions*," p.16, 21-22 October 2021.

[6] Ed. Storms, "A New and Improved Understanding of Cold Fusion Based on the Observed Behavior," Presentation at ICCF26, Morioka City, Japan, May 26-30, 2025.

[7] M. Miles, and P. L. Hagelstein, "Consistency of helium production with the excess power in the palladium-D_2O electrochemical system". *Journal of Electroanalytical Chemistry*, 2025. **977**: p. 118786.

[8] H. A. Bethe, and C. L. Critchfield, "The formation of deuterons by proton combination", *Phys. Rev*. **54** (1938) 248-254.

[9] S. E. Kooning, and M. Nauenberg, "Calculated fusion rates in isotopic hydrogen molecules", *Nature*, **339**, 690-691 June 1989 DOI: 10.1038/339690a0.

[10] A. Gonis, and W.H. Butler, Multiple Scattering in Solids, Springer-Verlag, New York,1999.

[11] R.R. Arons, Y. Tamminga, "On the Diffusion of H and D in Pd between 50 and 300° K," *Physica Status Solidi (B),* vol. 40, issue 1, pp. 107-112.

[12] P. L. Hagelstein, F. Metzler1, M. K. Lilley, J. F. Messinger1, and N. Galvanetto1, "Models for nuclear fusion in the solid state," arXiv:2501.08338v2.

[13] J. Kasagi, Y. Honda, K. Fang, Screening energy for low energy nuclear reactions in condensed matter, Cold Fusion-Advances in Condensed Matter Nuclear Science, Edited by Jean-Paul Biberian, Elsevier 2020, p.167-187.

[14] D. J. Nagel, "Potential Correlations between Apparent Peaks in LENR Transmutation Data and Deuteron Fusion Screening Data", *Journal of Condensed Matter Nuclear Science*, **39** (March 2024):295–321. https://doi.org/10.70923/001c.134019.

[15] J. B. Natowitz and R. L. Wolke, "Isomeric Cross Sections and Yield Ratios of (d, p) Reactions below 15 MeV", *Phys. Rev*. **155** (1967),1352-1361.